The 24th Computational Fluid Dynamics Symposium
Paper No.255

Numerical Simulation of Asymmetric Flow Past a Full Hull Form Under Strong Wall Effect

o Yoshiaki Kodama, National Maritime Research Institute, Tokyo, kodama@nmri.go.jp
Takanori Hino, National Maritime Research Institute, Tokyo, hino@nmri.go.jp
Kunihide Ohashi, National Maritime Research Institute, Tokyo, k-ohashi@nmri.go.jp

The stern flow of a 6m-long bulk carrier model placed in a tunnel of 2m x 0.88m rectangular cross section, became asymmetric due to strong wall effect, but recovered symmetry by setting a pair of flow liners at the corners of the section and thus reducing the wall effect. The *k-ω* SST turbulence model can reproduce the phenomena, while the Spalart-Allmaras model and he *k-ω* BSL model cannot. It has been confirmed that the result is not affected by grid resolution. A simple oblique towing method with an oblique angle of 0.1 degrees, whose magnitude is not important because it works as a trigger, has been found useful for testing the susceptibility or resistance of the flow to asymmetry.

1. Introduction

In order to improve loading efficiency, the hull forms of displacement-type ships such as tankers and bulk carriers are becoming more and more like a rectangular box. The block coefficient C_B defined by

$$C_B = \frac{[\text{displacement}]}{[\text{length}]\times[\text{width}]\times[\text{water depth}]} \quad (1)$$

, which indicates the boxiness or fullness of a hull form, takes slightly over 0.8 with conventional tankers, but exceeds 0.9 with newly sought Post-Panamax hull forms, which will be used in the enlarged Panama Canal.

The stern flow of hull forms of very large C_B tends to be unstable due to asymmetry of the flow, alternating sides in time. This phenomenon restricts the applicability of the hull form. Therefore, being able to predict flow asymmetry has practical importance.

The cavitation tunnel of NMRI has a rectangular test section whose dimensions are 8.0m length, 2.0m width, and 0.88m depth, in which a ship model of length up to 6m can be fixed to the top wall, so that cavitation tests can be carried out for a propeller operating in the wake of the model. However, since the wall effect is non-negligible, the wake at the propeller plane is not the same as that in the towing tank.

Fig.1(a) schematically shows a ship model slowly towed in a towing tank so that the wave effect is negligible. In case the model is installed in a rectangular test section after cutting it slightly above the waterline, as shown in Fig.1(b), the wall effect accelerates the flow past the model near the bow, and decelerates near the stern, resulting in thinning and thickening of the boundary layer on the model in the front half and rear half, respectively.

As shown in Fig.1(c), if an ideal flow liner, whose shape is equal to a stream tube surrounding the model in the towing tank, is installed in the test section, one should be able to cancel out the wall effect at least theoretically. Since the final goal is to test the propeller in the wake of a full-scale ship, whose length exceeds 300m, the thinning effect in the front half is useful because the full-scale boundary layer is thinner than that of the model scale. Therefore, it is a standard procedure (1) to measure the wake distribution at the propeller disk in the towing tank, (2)to estimate the full-scale wake distribution using a suitable estimation method such as the Sasajima-Tanaka's method[1], and to make the wake distribution measured in the tunnel as close as possible to the estimated distribution by changing the size and the streamwise location of a pair of flow liners fixed at the lower corners of the test section in the stern area, as shown in Fig.1(d).

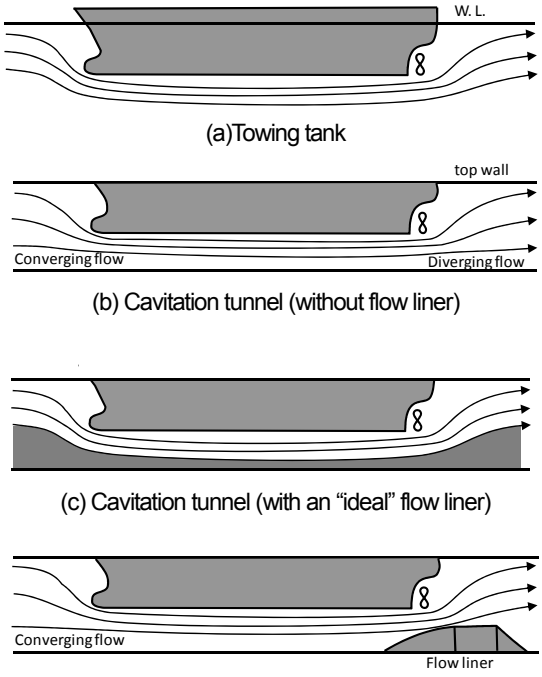

(a)Towing tank

(b) Cavitation tunnel (without flow liner)

(c) Cavitation tunnel (with an “ideal” flow liner)

(d) Cavitation tunnel (with a real flow liner)

Fig.1 Wall effect in the cavitation tunnel and its reduction using a pair of flow liners.

In case the wall effect in the cavitation tunnel is strong, the stern flow sometimes becomes asymmetric, in spite of the geometrical symmetry of the model and the tunnel wall. Then the use of flow liners works to recover the flow symmetry. In reality, the

model geometry and the upstream flow are not symmetric because of manufacturing and setting errors, and somehow it is always the starboard side (the right side if seen from downstream) where the stern flow is slower in the cavitation tunnel of NMRI.

In this paper, the SR174B4 ship model[2], a research hull form modeling a bulk carrier is used as a test case. It has the length L_{pp}=6.0m, the width B=0.92m, and the block coefficient C_B=0.824. The wake of the model is symmetric in the towing tank, asymmetric in the cavitation tunnel without flow liners, and symmetric again with the use of flow liners[2].

It is a challenging test for CFD whether it can simulate thinning and thickening of the boundary layer and the formation of asymmetrical flow past a geometrically symmetrical body, both due to the wall effect. As to the thinning and thickening phenomena, Kodama et al.[3] computed flows past the same ship model using the Modified Spalart-Allmaras turbulence model[4] and a single-side grid assuming symmetry, and obtained good correlation between measured and computed wake distributions.

The formation of asymmetrical flow past a geometrically symmetrical body is more challenging to CFD. it should be noted that, in actual computations, although body geometry can be made symmetric with machine accuracy, solution-updating using a relaxation method can trigger flow asymmetry through directional sweeps and insufficient convergence at each time step.

2. CFD solver

The CFD solver used is SURF[7](version 6.43), an incompressible flow solver for ship flows, based on the pseudo-compressibility approach on unstructured grids. Incompressibility of the computed flow is satisfied only at convergence. The solver uses the point Gauss-Seidel relaxation method for updating the solution.

All the computations were started from the zero-flow state everywhere, then increasing the u-component uniformly at each time step until the 100th time step. The pseudo-compressibility parameter β was 1.0. The local time-stepping was used with the local Courant number CFL=5.0, but sometimes the CFL was reduced to 2.0 to get convergence. No sub-iteration was applied at each time step. Ref.(3) used the same solver with the same parameters.

3. Turbulence models

Four kinds of turbulence models were used.

(1)Spalart-Allmaras model (SA)[4]

The model is based on the transport equation for the kinematic eddy viscosity ν_t (more precisely $\tilde{\nu}$, a variant of ν_t), which is tuned for free shear layers and wall boundary layers in laminar and turbulent regimes. In the boundary layer in adverse pressure gradient, it gives larger ν_t than experiment, which is also the case with conventional turbulence models such as the Cebeci-Smith model and the standard k-ε model.

(2)Modified Spalart-Allmaras model (MSA)[5]

In the model, the production term for ν_t is made smaller in a region where, as in the vortex core, the strain rate tensor is smaller than the vorticity. The model is known to produce good results in the ship stern flow where there is a pair of strong longitudinal vortices.

(3) k-ω BSL model (KOBSL)[6]

In order to avoid strong sensitivity of the original k-ω model on the free-stream ω value, Menter combined the original k-ω model and the standard k-ε model, in which the original k-ω model is used in the inner layer while the standard k-ε model is used in the outer layer, so that the unwanted sensitivity is avoided.

(4) k-ω SST model (KOSST)[5]

Menter further modified the k-ω BSL model to develop the k-ω SST model, in which ν_t satisfies the Bradshaw's assumption that the shear stress in a boundary layer is proportional to the turbulent kinetic energy k. This modification results in substantially decreased values of ν_t in adverse pressure gradient zones.

The actual equation forms are as follows, with τ being the Reynolds shear stress and Ω being the absolute value of vorticity. The original form of the kinematic eddy viscosity is

$$\nu_t = \frac{k}{\omega}, \tag{2}$$

The Bradshaw's assumption is in the form

$$\frac{\tau}{\rho} = a_1 k, \tag{3}$$

whereas, in two-equation models, the Reynolds shear stress is expressed as

$$\frac{\tau}{\rho} = \nu_t \Omega. \tag{4}$$

In the k-ω SST model, the kinematic eddy viscosity is defined as

$$\nu_t = \frac{a_1 k}{\max(a_1\omega; F_2\Omega)} \tag{5}$$

$$F_2 = \tanh(\arg_2^2) \tag{6}$$

$$\arg_2 = \max\left(2\frac{\sqrt{k}}{0.09\omega y} \quad \frac{500\nu}{y^2\omega}\right). \tag{7}$$

In the inner layer, arg2 becomes very large, and F_2 becomes unity. Then eq.(5) reduces to

$$\nu_t = \frac{a_1 k}{\Omega}, \tag{8}$$

which produces eq.(3) by substituting into eq.(4).

In the outer layer, arg2 goes to zero, and so is F_2. Then eq.(5) reduces to eq.(2), i.e. the original form.

Hino[8] computed flows past a tanker form using SURF with the k-ω SST turbulence model.

4. Grid

(1)Grid topology and resolution

Grids have the H-O topology, covering both sides of the ship hull. The grid coordinates are normalized by the ship length L_{pp} (length between perpendiculars) with the origin at midship center. The bottom boundary consists of the front cut, the hull surface, and the rear cut. The top boundary is the outer boundary, which consists of a half cylinder of radius 1.5, or the cavitation tunnel wall, or the tunnel wall with a pair of flow liners as a part of it. In the latter

two cases, the grid was clustered toward the top boundary as well, with the minimum spacing being 0.001 and the free-slip boundary condition being imposed. The left and right boundaries consist of the z=0 symmetry plane, simulating the free surface or the top wall of the tunnel. The upstream and downstream boundaries are located at x=-1.5 and x=1.5. The Dirchlet boundary condition for pressure, i.e. p=0.0, was imposed at the downstream boundary.

Most computations have been carried out using the standard grid (StdG), whose number of grid points are 131*89*61 in the I(upstream-downstream), J (girthwise), and K (bottom-top) directions. The minimum spacing is $0.35*10^{-6}$.

For the grid resolution study, the fine grid (FineG), whose number of grid points is 191*133*91, has been used. The grid resolution has been made 1.5 times in all the three directions in the rear half, while keeping the minimum spacing unchanged.

The flow liners used are FL2[(2)], which have the cylindrical parallel part of radius 0.44m and length 0.6m with front (1.1m length) and rear (0.5m length) conical parts. In the computation, the rear conical part has been made three times longer than real, in order to stabilize the computation.

Fig.2 shows the surface grids. The propeller disk is at x=0.4888 with the radius 0.0205.

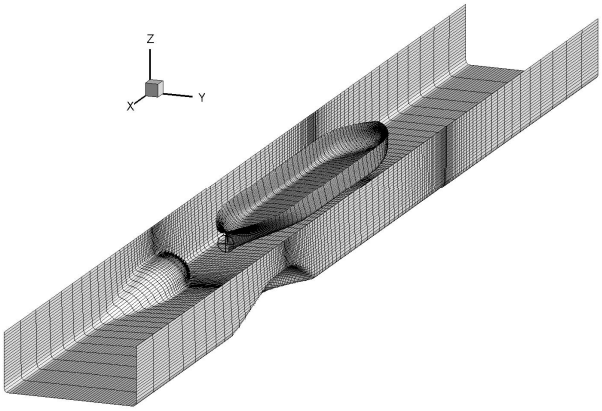

(a)Hull surface and tunnel wall grids with flow liners (StdG)

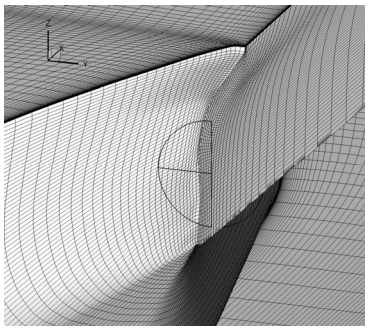

(b)Stern grid with the propeller disk(FineG).

Fig.2 Surface grids

(2)Hull surface grid rotation

We have found out that computing the flow by rotating the hull surface only slightly about the hull center is a good test for the susceptibility of the flow to asymmetry. As shown in Fig.3, the bottom surface grids are shifted first. The hull surface grid is rotated by the angle θ, then the grid points on the two cuts are shifted accordingly. The grid points on the top boundary are unchanged. The grid points between the two boundaries are shifted by linear interpolation based on the distance. The rotation angle θ is 0.1 or 0.2 degrees. The rotation θ =0.1 deg. causes the y-shift of +1cm at the stern end of a 6m-long ship model.

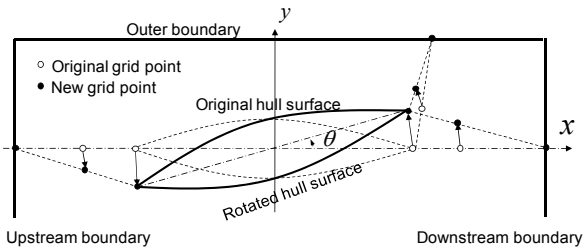

Fig.3 Hull surface grid rotation by angle θ

4. Towing tank (rad1.5)

The model with turbulence stimulators at the bow was towed in a towing tank, whose width is 18m and the water depth is 7m. The towing speed was 1.35m/s, resulting in the Froude number F_n=0.176 and the Reynolds number R_e=$8.28*10^6$.

Fig.4 shows the measured velocity distribution at the propeller plane (x=0.4888)[(2)], looked from behind, where the u-component is normalized by the towing speed. Since there is a pair of longitudinal vortices of opposite sign in the wake, the contour lines exhibit a so-called "hook" shape. The bulge of the slow speed zone at the center is caused not only by the induced velocities of the longitudinal vortices but also by the shaft housing for the model propeller.

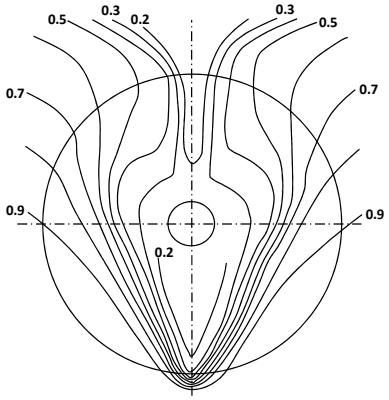

Fig.4 Measured towing tank wake at propeller plane

Fig.5 shows the computed flow field using StdG and KOSST. The water surface was approximated as the symmetry plane, because the corresponding Froude number is low enough to neglect the free-surface wave effect. The cylindrical outer boundary is at the radius 1.5 (Rad1.5), which assures the wall effect being negligibly small. The Reynolds number is R_e=$8.28*10^6$, the k-ω SST turbulence model, and the standard grid.

Fig.5(a) shows the contour lines in case the rotation angle θ =0.0 deg.. They are symmetrical and show reasonable agreement with the measurement, except that the u=0.9 line is significantly wider and that the slow speed bulge is smaller. It should be noted that the grid resolution is not sufficient and the shaft housing is not taken into account in the computation.

Fig.5(b) shows the rotation angle θ =0.1 deg. case. The low

speed bulge is slightly shifted toward left.

Fig.5(c) shows the hull surface pressure at the stern. It also shows the u=0 line, denoting the separation zone.

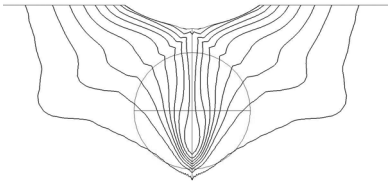

(a)Wake at propeller plane (θ =0.0 deg.)

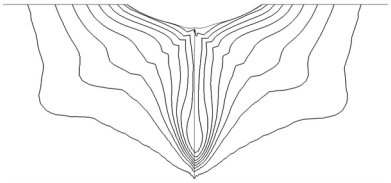

(b)Wake at propeller plane (θ =0.1 deg.)

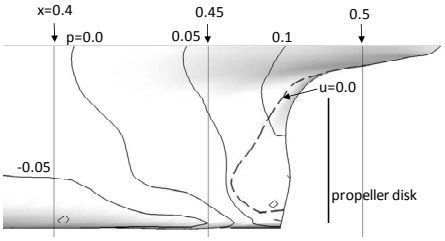

(c)Stern surface pressure

Fig.5 Computed flow field (Rad1.5, StdG, θ =0.0 deg., KOSST)

5. Cavitation tunnel without flow liners (no FL)

The same ship model was fixed to the top wall of the cavitation tunnel, after cutting it slightly above the water plane. The average flow speed in the test section was 3.8m/s corresponding to R_e=1.97*10^7. Fig.6 shows the measured u-contours at the propeller plane, normalized by the maximum value inside the propeller disk. The pattern shows strong asymmetry, the right side being slower.

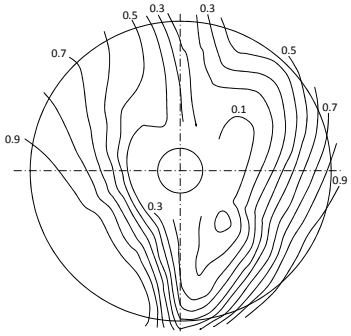

Fig.6 Measured cavitation tunnel wake at propeller plane (no FL)

In case the modified Spalart-Allmaras turbulence model was used, the computed flow in the θ =0.0 deg. case showed stern flow separation on alternating sides, and did not converge. Fig.7 shows the time history of the side force C_y.

Fig.7 Time history of C_y in the cavitation tunnel (no FL, StdG, θ =0.0 deg., MSA)

Figs.8(a),(b),(c) show the wake distribution at the propeller plane (x=0.4888) at θ =0.0, 0.1, and 0.2 deg. The distributions are very similar to each other and asymmetric, the left side being slower, opposite to the measured result. Fig.8(d) shows the distribution at θ = - 0.1 deg., which is anti-symmetric with the previous three. These results suggest that the stern flow is highly susceptible to asymmetry and that only a small bias triggers the asymmetry.

Figs.8(e),(f) show the surface pressure distribution and the separation zone (u<0.0) at the stern. At first the surface pressure is lower than that of the unbounded case, because of the flow acceleration up to midship, but the recovery toward the stern end is more rapid. In agreement with the flow asymmetry, the distributions are asymmetric.

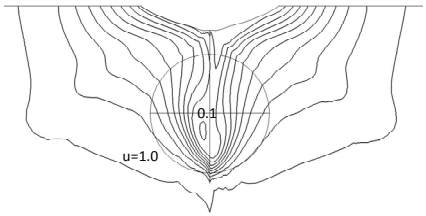

(a)Wake at propeller plane (θ =0.0 deg.)

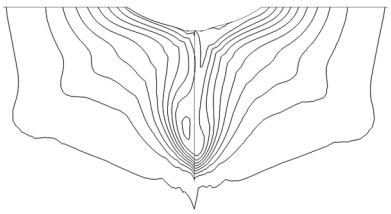

(b)Wake at propeller plane (θ =0.1 deg.)

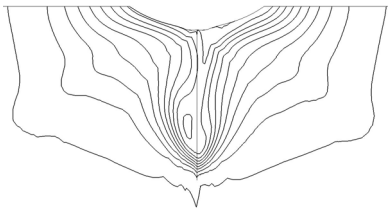

(c)Wake at propeller plane (θ =0.2 deg.)

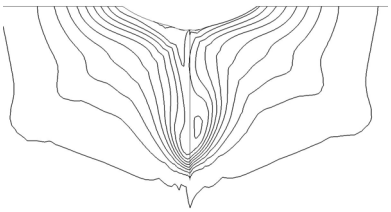

(d)Wake at propeller plane (θ =-0.1 deg.)

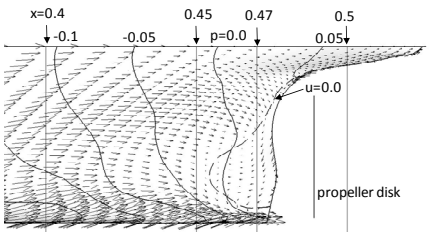

(e)Stern surface pressure (left side, θ =0.0 deg.)

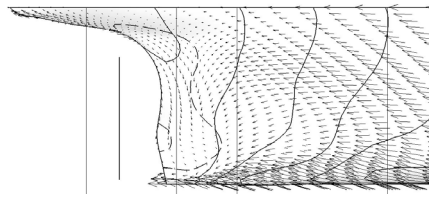

(f)Stern surface pressure (right side, θ =0.0 deg.)

Fig.8 Computed flow field in the cavitation tunnel (no FL, StdG, KOSST)

Figs.9(a),(b) show the wake distributions at the propeller plane in case the fine grid (FineG) is used. By comparing Fig.8(b) and Fig.9(b), it is seen that the grid refinement makes the slow region even slower and wider, while maintaining the overall character. As shown in Fig.9(a), the t θ =0.0 case of the fine grid gives the slow region on the right, in contrast to the standard grid case. In summary, it may be stated that the θ =0.0 case gives the distribution very close to either the θ =0.1 case or the θ = - 0.1 case, which are anti-symmetric.

Fig.9(c) shows the wake distribution at the propeller plane (θ =0.0), normalized by the maximum value in the propeller disk (u_{max}=0.98). By comparing the figure with Fig.6, it is seen that the computed result shows reasonable agreement with the measurement.

Fig.9(d) shows the wake distribution plus the velocity vectors on the plane. A pair of longitudinal vortices are clearly seen with the center of the left one being lower than the right one, causing the asymmetric wake distribution.

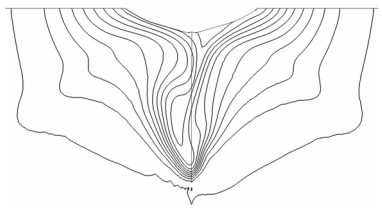

(b)θ =0.1 deg.

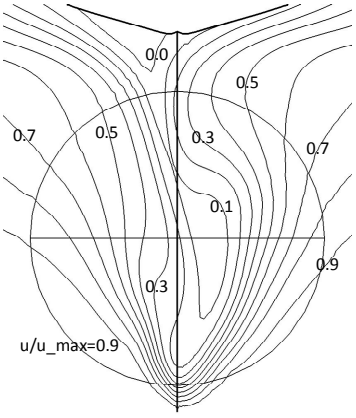

(c)θ =0.0 deg.(u_{max}=0.98)

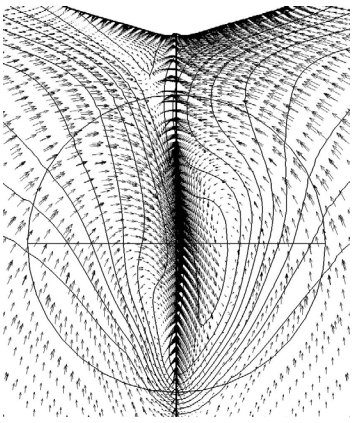

(d)θ =0.0 deg.(u_max=0.98, vectors)

Fig.9 Computed cavitation tunnel wake at propeller plane (no FL, FineG, KOSST)

Figs.10(a),(b) show the wake distributions at the propeller plane in case the Spalart-Allmaras turbulence model is used. In case θ =0.0 deg., the converged flow is highly symmetric, which is in contrast to the *k-*ω SST turbulence model case. As shown in Fig.10(b), the rotation by 0.1 degrees causes asymmetry only slightly.

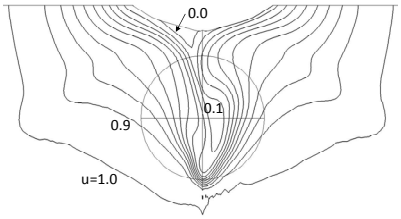

(a)θ =0.0 deg.

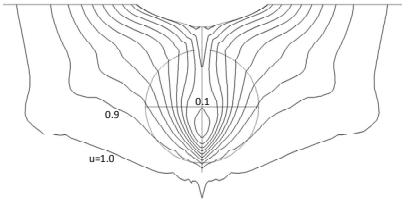

(a)θ =0.0 deg.

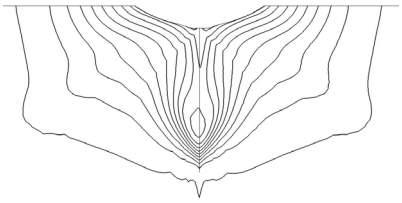

(b)θ =0.1 deg.

Fig.10 Computed cavitation tunnel wake at propeller plane (no FI, StdG, SA)

The results using the *k*-ω BSL turbulence model, shown in Fig.11(a),(b) are similar to that of SA, i.e. the model fails to predict flow asymmetry. By comparing it with those of the *k*-ω SST turbulence model shown in Fig.8, it is amazing that such a small modification as eq.(5) significantly improves the capability of the turbulence model.

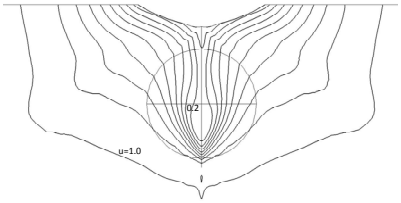

(a)θ =0.0 deg.

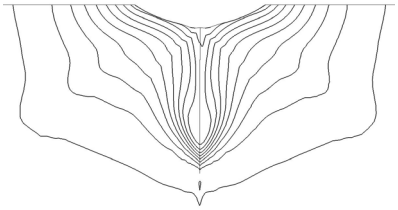

(b)θ =0.1 deg.

Fig.11 Computed cavitation tunnel wake at propeller plane (no FI, StdG, KOBSL)

Figs.12, 13, 14 show the comparison of the wake and the kinematic eddy viscosity ν_t distributions using the KOSST, the KOBSL or the SA turbulence model at x=0.47 and x=0.4888(propeller plane). At x=0.47, where there is flow separation, the ν_t distribution is slightly asymmetric with KOSST, and symmetric with KOBSL and SA, in agreement with the tendency in the wake. In general, the ν_t value is the smallest with KOSST. With SA, the ν_t distribution is more confined toward the hull surface than the other two.

At x=0.4888 (propeller plane), the ν_t distribution is highly asymmetric with KOSST, and almost symmetric or symmetric with KOBSL and SA. With KOSST, the large ν_t zone corresponds to the high wake zone. There are sharp peaks on the symmetry plane in the distribution of KOBSL. In the computation, the residual showed occasional bursts, and therefore they are regarded as local numerical oscillation. SA gives the most symmetrical distributions.

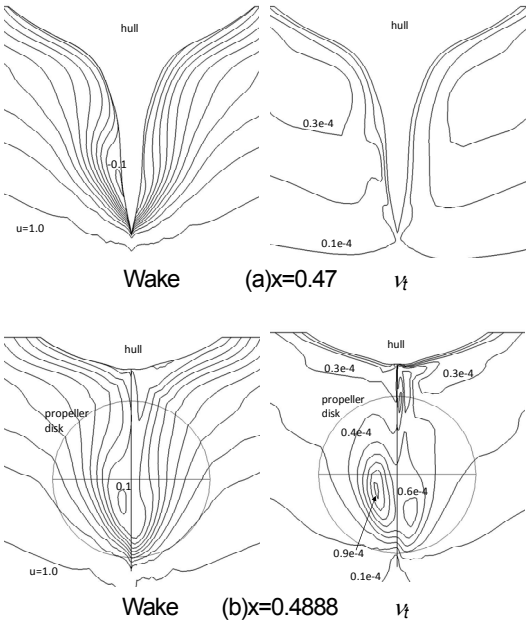

Fig.12 Computed contours(StdG, no FL, θ =0.0 deg., KOSST)

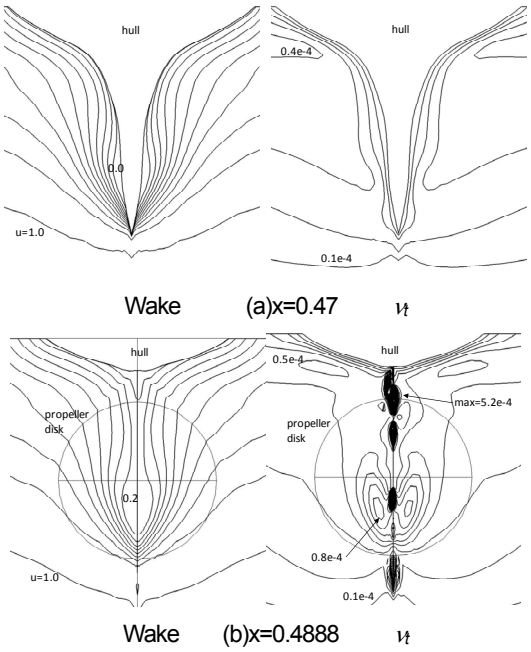

Fig.13 Computed contours(StdG, no FL, θ =0.0 deg., KOBSL)

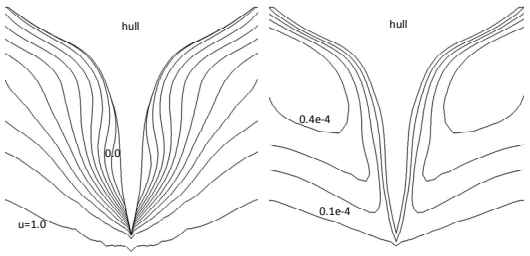

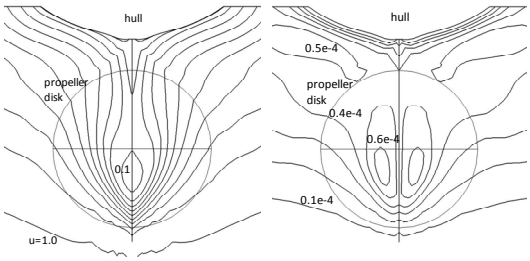

Wake (b)x=0.4888 ν_t

Fig.14 Computed contours(StdG, no FL, θ =0.0 deg., SA)

6. Cavitation tunnel with flow liners

Fig.15 shows the measured wake distribution at the propeller plane in case the flow liners are installed in the cavitation tunnel. The distribution is normalized by the maximum u-value in the propeller disk. The distribution has regained symmetry, using the flow liners. It should be noted that the wake region is thinner than that in the towing tank, because it simulates the estimated full scale wake.

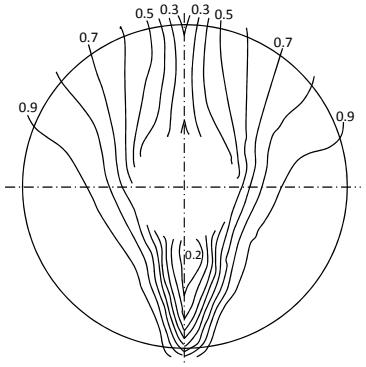

Fig.15 Measured cavitation tunnel wake at propeller plane (FL2). Normalized by the maximum value.

Figs.16(a),(b) show the computed wake distribution at the propeller plane using the standard grid and the *k-ω* SST turbulence model. In agreement with the measurement, the flow is symmetric at θ =0.0 deg.. The flow is highly resistant to asymmetry, as the θ =0.1 deg. case shows.

Fig.16(c) shows the hull surface pressure distribution at the left stern. The pressure recovery in the downstream direction is slow because of the flow acceleration caused by the flow liners. The flow acceleration also causes a low pressure zone along the hull bottom. Due to this, the wake distribution shows a sharp peak at the bottom. The separation zone is hardly affected by the flow liners.

Fig.16(d) shows the wake distribution normalized by the maximum value in the propeller disk. The distribution agrees well with the measurement.

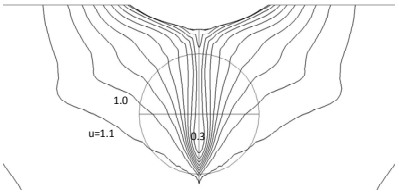

(a) Wake at propeller plane (θ =0.0 deg.)

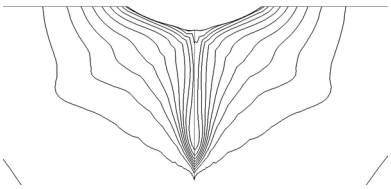

(b) Wake at propeller plane (θ =0.1 deg.)

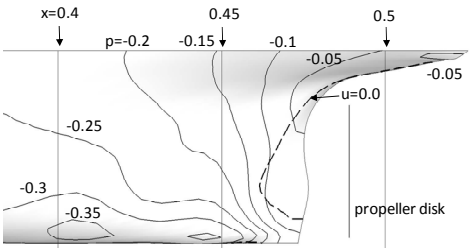

(c)Left stern surface pressure(θ =0.0 deg.)

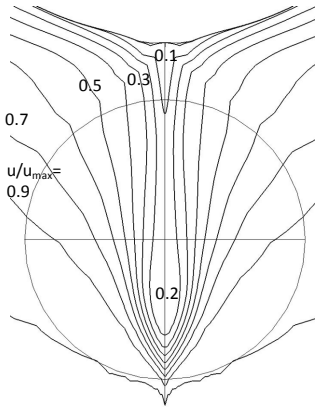

(d)Wake at propeller plane(θ =0.0 deg., u_{max}=1.113)

Fig.16 Computed flow field in the cavitation tunnel(FL2, StdG, KOSST)

Fig.17(a) shows the distributions of the maximum non-dimensional pressure as a function of x. In the no-FL and FL2 cases, due to the wall effect, the hull surface pressure in the parallel part is significantly lower than the Rad1.5 case. Also, Fig.17(c) shows that the boundary layer at x=0.0 is significantly thinner.

In the stern part, the no FL case gives steeper adverse pressure gradient and larger pressure rise than the Rad1.5 case. That is perhaps why the flow asymmetry occurs in the no FL case. In the FL2 case, the flow acceleration due to the flow liners retards the pressure rise. Once the pressure rise starts, it is gradual in the beginning, followed by an even steeper one than that of the no FL case. But it does not last long, and the resultant pressure rise is smaller than that of the no FL case. These two effects might be the reason why the flow asymmetry disappears by using the flow liners.

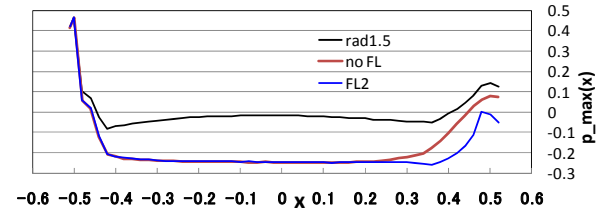

(a)p_{max}(x) on hull surface

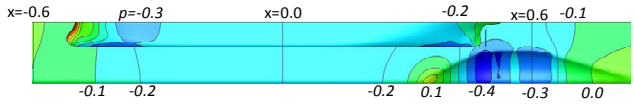

(b)Pressure on hull surface and top boundary (right half, FL2)

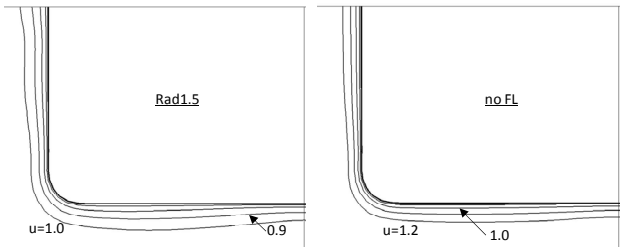

(c)u-contours (x=0.0)

Fig.17 Effects of tunnel wall and flow liners on the surface pressure and u-contours (StdG, θ =0.0 deg., KOSST)

7.Conclusions

The stern flow of a 6m-long bulk carrier model placed in a tunnel of 2m x 0.88m rectangular cross section, became asymmetric due to strong wall effect, but recovered symmetry by setting a pair of flow liners at the corners of the section and thus reducing the wall effect.

The use of the modified Spalart-Allmaras model did not show convergence for the case without flow liners.

The *k-ω* SST turbulence model can reproduce the phenomena (flow symmetry or asymmetry), while the Spalart-Allmaras turbulence model and the *k-ω* BSL turbulence model always produce symmetrical flows. The clear distinction between the results by the *k-ω* BSL and the *k-ω* SST models shows that the modification based on the idea that shear stress in a boundary layer is proportional to the turbulent kinetic energy k is essential to simulating the flow asymmetry. It has been confirmed that this result is not affected by the grid resolution.

The combination of the *k-ω* SST turbulence model and a simple oblique towing method, in which the hull form is rotated by a small angle θ (typically θ=0.1 degrees), has been found useful for testing the susceptibility or the resistance of the flow to asymmetry. In case the wake distribution is asymmetric at θ=0.0 deg., it agrees either with the θ=0.1 deg. case or with the θ= - 0.1 deg. case. Doubling the rotation angle to θ=0.2 deg. hardly affects the wake distribution, which suggests that rotating a hull by a small angle works as a trigger to flow asymmetry, and the magnitude of the rotation angle is unimportant. In case the wake distribution is symmetric at θ=0.0 deg., the case θ=0.1 deg. shows the degree of susceptibility or resistance of the flow to asymmetry.

Acknowledgments

The authors thank the Japan Ship Technology Research Association for giving permission to use the SR174B4 hull form, and Dr. Yoshitaka Ukon of NMRI for providing the measurements.

Bibliography

(1) Tanaka, I., "Scale Effects on Wake Distribution and Viscous Pressure Resistance of Ships," J. of the Society of Naval Architects of Japan, Vol. 146 (1979), pp. 53-60.

(2) Ukon, Y., Fujisawa, J., Kodama, Y., Hinatsu, M., and Kurobe, Y., "Wake Simulation and Cavitation Experiment on a Full Ship Model with Flow Liners," Conference Proceedings of the Japan Society of Naval Architects and Ocean Engineers, Vol. 9E (2009), pp. 107-110 (in Japanese).

(3) Kodama, Y., Hino, T., Ukon, Y., and Hinatsu, M., "Numerical Simulation of Wall Effect Reduction Using Flow Liners in a Cavitation Tunnel," J. of the Japan Society of Naval Architects and Ocean Engineers, Vol. 11 (2010), pp. 81-90 (in Japanese).

(4) Spalart, P. R. and Allmaras, S. R.," A One-Equation Turbulence Model for Aerodynamics Flows," La Recherche Aerospatiale, 1994, No.1, pp.5-21.

(5) Hirata, N. and Hino, T.: A Comparative Study of Zero- and One-Equation Turbulence Models for Ship Flows, J. of the Kansai Society of Naval Architects Japan, Vol. 234 (2000), pp.17-24.

(6) Menter, F.R., "Two-Equation Eddy-Viscosity Turbulence Models for Engineering Applications," AIAA Journal, vol.32, No.8 (1994), pp.1598-1605.

(7) Hino T., "A 3D Unstructured Grid Method for Incompressible Viscous Flows," J. of the Soc. Naval Archit. Japan, Vol.182 (1997), pp.9 - 15.

(8) Hino, T., "Navier-Stokes Computations of Ship Flows on Unstructured Grids," The Proceedings of the 22nd Symposium on Naval Hydrodynamics, Washington, D.C. (1998), pp.463-475.